Formation and Annihilation of Vortex-Antivortex Pairs by Magnetic Dipoles in a Mesoscopic Superconducting Film

L. Peng[a,*], Y. Wang[a], J. Xu[b], Y. Zhang[a], L. Zhou[b], Y. Zhu[a] and C. Cai[c]

[a]Department of Physics, Shanghai University of Electric Power, Shanghai 201300, China

[b]Shanghai Institute of Space Power-Sources, Shanghai 200245, China

[c]Shanghai Key Laboratory of High Temperature Superconductors, Physics Department, Shanghai University, 99 Shangda Road, Shanghai 200444, China

(Received July 31, 2019; revised version August 22, 2019; in final form September 5, 2019)

Using a finite element method to numerically solve the time-dependent Ginzburg-Landau equations, we study the vortex-antivortex dynamics in a hybrid structure consisting of a finite size superconducting film with two magnetic dipoles on top which generate vortices and antivortices in the presence of a external homogeneous magnetic field. We obtain the different vortex-antivortex patterns for different arrangement and magnetic moments of two magnetic dipoles. Our results provide a tool for an effective manipulation of magnetic flux in mesoscopic hybrid structures.

DOI: 10.12693/APhysPolA.136.962

PACS/topics: vortices and antivortices, magnetic dipoles, The time-dependent Ginzburg–Landau equations, finite element method

1. Introduction

The possibility of manipulating vortex matter by using various pinning centers is of significant importance for possible applications in nano- and micro-devices [1–8]. In a homogenous superconductor, in the presence of a homogenous external magnetic field, the direction of the vortex motion in the superconductor is well defined. The situation will change if inhomogeneities are present in the superconductor. They can be either of intrinsic nature or artificially created arrays of antidots (or arrays of magnetic particles) [9–13]. Magnetic dots with strong magnetization can create vortices or pairs of vortices in the superconductor [6–8], which give rise to a variety of nontrivial effects and novel stable V-Av configurations in superconducting films. The study of those systems opens the way to manipulate the vortex patterns.

Experimentally the V–Av state has been found [14–15]. However, there still exists a need for alternative proposals of different systems. Due to the magnetic nature of the magnetic dipoles, pinning effects can be significantly enhanced in superconducting films, which, in addition, provide a unique opportunity to tune field-induced superconductivity by changing the magnetic state of the magnetic dipoles. In this paper we study flux guidance in a hybrid structure consisting of a finite-size superconducting film with two magnetic dipoles on top. Our aim is to study the vortex-antivortex guidance by varying the external magnetic field and the magnetization and position of the magnetic dipoles. As a theoretical approach we use time-dependent Ginzburg–Landau (TDGL) equations because they allow to study both the nucleation of the V-Av pairs and their dynamics. Meanwhile, by using finite-element method (FEM) [16–20] the TDGL equations are numerically solved. The high precision of the finite-element method in solving linear equations allows us to significantly increase the grid resolution, for instance, in the neighborhood of the V–Av molecule. The use of triangular finite elements proved as a more accurate treatment of the sample geometry than we could achieve with a rectangular grid, for any arbitrary sample geometry.

*corresponding author; e-mail: plpeng@shiep.edu.cn

2. Time-dependent Ginzburg–Landau method

We consider a thin-film square-shaped superconductor sample with lateral sizes $L_x = L_y$ and thickness d_s (see Fig. 1). The Ginzburg-Landau theory describes the superconducting state through a complex order parameter ψ for which $|\psi|^2$ represents the density of Cooper pairs. The order parameter and the local magnetic field can be determined by the TDGL equations, which are expressed by

$$\left(\frac{\partial}{\partial t} + \mathrm{i}\Phi\right)\psi = -\left(-\mathrm{i}\nabla - \boldsymbol{A}\right)^2\psi + (1 - |\psi|^2)\psi, \quad (1)$$

$$\sigma\left(\frac{\partial \boldsymbol{A}}{\partial t} + \nabla\Phi\right) = \boldsymbol{J}_s - \kappa^2\nabla\times\nabla\times\boldsymbol{A}, \quad (2)$$

with boundary conditions

$$\boldsymbol{n}\cdot\left(-\mathrm{i}\nabla - \boldsymbol{A}\right)\psi|_{\perp,\mathrm{boundary}} = 0, \quad (3)$$

where Φ is the electric potential, $\boldsymbol{A}$ is the vector potential, σ is the electric conductivity, $\boldsymbol{n}$ is the normal unit vector on the surface. The density of the superconducting current $\boldsymbol{J}_s$ is,

$$\boldsymbol{J}_s = \mathrm{Im}(\psi^*\nabla\psi) - \boldsymbol{A}|\psi|^2. \quad (4)$$

The vector potential $\boldsymbol{A}$ can be represented as $\boldsymbol{A} = \boldsymbol{A}_m + \boldsymbol{A}_1$, where $\boldsymbol{A}_m$ corresponds to the magnetic field $\boldsymbol{B}_{mz}$, induced by the two magnetic dipoles (the magnetic moment $\boldsymbol{m}$), and $\boldsymbol{A}_1$ denotes the vector potential corresponding to an additional external homogeneous magnetic field $\boldsymbol{B}_1$, which may be applied to the system. Vector potential of the external homogeneous magnetic field (along the z-axis) is expressed by,

$$\boldsymbol{A}_{B_1} = \frac{[\boldsymbol{B}_1, \boldsymbol{r}]}{2} = \Big(-\frac{B_z y}{2}\Big)\boldsymbol{i} + \Big(\frac{B_z x}{2}\Big)\boldsymbol{j} + 0\,\boldsymbol{k}. \quad (5)$$

Vector potential of a out-of-plane magnetic dipole (along the z-axis) is expressed by,

$$\boldsymbol{A}_0 = \frac{[\boldsymbol{m}, \boldsymbol{r}]}{r^3} = \Big(-\frac{m_z y}{r^3}\Big)\boldsymbol{i} + \Big(\frac{m_z x}{r^3}\Big)\boldsymbol{j} + 0\,\boldsymbol{k}, \quad (6)$$

where m_z denotes the magnitude of the magnetic moment in the z-direction (normal to the film surface), and the corresponding magnetic field is as follows,

$$\boldsymbol{B} = \Big(-\frac{\partial A_y}{\partial z}\Big)\boldsymbol{i} + \Big(\frac{\partial A_x}{\partial z}\Big)\boldsymbol{j} + \Big(\frac{\partial A_y}{\partial x} - \frac{\partial A_x}{\partial y}\Big)\boldsymbol{k}. \quad (7)$$

The out-of-plane component of the magnetic field has a large impact on the order parameter in the superconducting film, and therefore we may neglect the in-plane magnetic field. The out-of-plane component is,

$$B_z = m_z \frac{2z^2 - x^2 - y^2}{r^5}, \quad (8)$$

where $r = \sqrt{x^2 + y^2 + z^2}$. We scale the length in units of $\xi = \hbar/\sqrt{2m\alpha_0}$, the order parameter ψ in units of $\psi_0 = \sqrt{-\alpha_0/\beta}$ (with α_0 and β being the GL coefficients [16]), the vector potential $\boldsymbol{A}$ in units of $A_0 = \sqrt{2}\kappa H_c \xi$, the time t in unit of $t_0 = \pi\hbar/(8k_B T_c)$, and the local magnetic field B and B_1 in units of $H_{c2} = \sqrt{2}\kappa H_c$, where H_c is the thermodynamical critical field, and $\kappa = \lambda/\xi$ is the GL parameter. We scale the m_z in units of $m_0 = \Phi_0\xi/(2\pi)$, where Φ_0 is quantum of the magnetic flux. The free energy of the superconducting state, measured in $F_0 = H_c^2 V/(8\pi)$ units, is expressed as

$$F = \frac{2}{V}\int \Big[-|\psi|^2 + \frac{1}{2}|\psi|^4 + |(-\mathrm{i}\nabla - \boldsymbol{A})\psi|^2 + \kappa^2(\boldsymbol{B} - \boldsymbol{H})^2\Big]\,\mathrm{d}V. \quad (9)$$

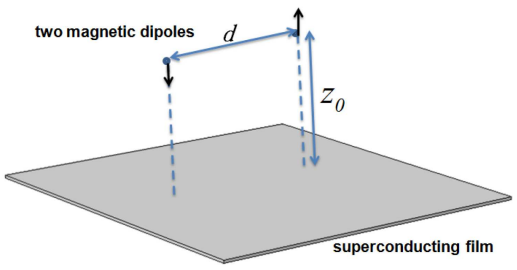

Fig. 1. A sketch of the envisioned experimental setup. Two point-like out-of-plane magnetic dipoles separated by a distance d and placed at a distance from the top surface of the superconducting film. A magnetic dipole has magnetic moment $\boldsymbol{m}$.

The transport current is introduced via the boundary condition for the vector potential in the x direction: $\nabla \times \boldsymbol{A}|_z\,(x = 0, w) = H \pm H_I$. The external dc current I is induced by imposed $H_I = 2\pi I/c$ on the lateral edges of the sample. The applied current density is given in units of $j_0 = \sigma_n\hbar/(2e\tau_{\mathrm{GL}}\xi)$ is the normal-state conductivity). Notice that the TDGL equations are gauge invariant under the transformations $\psi' = \psi\mathrm{e}^{\mathrm{i}\chi}$, $\boldsymbol{A}' = \boldsymbol{A} + \nabla\chi$, $\Phi' = \Phi - \frac{\partial\chi}{\partial t}$. So, we choose the zero-scalar potential gauge, that is, $\Phi = 0$ at all times and positions. The normalized time t/t_0 ranges from $t/t_0 = 0$ to $t/t_0 = 10^5$ for the evolution of the dynamics.

3. Results and discussions

We focus on the case when the magnetic fields of the two dipoles are strong enough to create V-Av pairs in a thin superconductor film. The vector potential $\boldsymbol{A}_m$ is sum of the vector potentials of two point-like out-of-plane magnetic dipoles separated by a distance d and placed at a distance from the top surface of the superconducting film. We assume that the thickness of the superconducting film d_s is smaller than the coherence length ξ and penetration depth λ, and therefore we can neglect the influence of the screening on $\boldsymbol{A}$. Our simulations have been carried out by using $\sigma = 1$,$\kappa = 1.2$, $L_x = L_y = 12\xi$. To begin with, we focus on the case, when the $z_1 = z_2 = 2\xi$. The distance between the out-of-plane point-like dipoles is $d = 6\xi$ for the system. As it is obvious from the definition of the used dimensionless parameters, the same set of these parameters can correspond to structures with different sizes depending on ξ and λ of the superconducting film. For the sake of contrast, we consider two cases: two dipoles are placed along x-axis and along diagonal line, respectively. In more detail, one magnetic dipole is magnetized in the negative z-direction and located at site (-3, 0, 2), and another is magnetized in the positive z-direction and located at site (3, 0, 2) for the arrangement along the x-axis. One magnetic dipole is magnetized in the negative z-direction and located at site $(-\frac{3\sqrt{2}}{2}, \frac{3\sqrt{2}}{2}, 2)$, and another is magnetized in the positive z-direction and located at site $(\frac{3\sqrt{2}}{2}, -\frac{3\sqrt{2}}{2}, 2)$, for the arrangement along the diagonal line. Figure 2 shows the z-component of the magnetic field ($B_{mz}(x, y = 0, z = 0)$) for the arrangement along the diagonal line (Fig. 2a) and along the x-axis (Fig. 2b), respectively. The insets show the magnetic field profile in the superconducting plane induced by the magnetic dipoles. Provided that the thickness of the superconducting film is small, the structure of the vortex and antivortex is mainly determined by an inhomogeneous two-dimensional distribution of the magnetic field of the magnetic dipoles. Figure 3 shows the number of V–Av pairs and free energy as a function of magnetic moments of the magnetic dipoles. Different lines with symbols represent the dependence for different arrangements of two magnetic dipoles. With increasing magnetic moment, the number of V–Av pairs increases from $N_{V-Av} = 0$

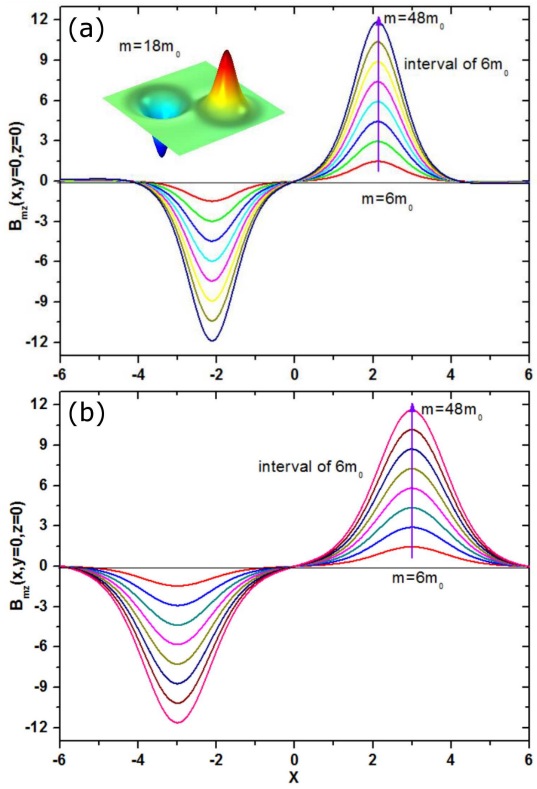

Fig. 2. (a) The z-component of the magnetic field $B_z(x, y = 0, z = 0)$ in the superconducting plane induced by two magnetic dipoles. A magnetic dipole is located at site $(-\frac{3\sqrt{2}}{2}, \frac{3\sqrt{2}}{2}, 2)$, and another is located at site $(\frac{3\sqrt{2}}{2}, -\frac{3\sqrt{2}}{2}, 2)$. The insets show the magnetic field profile in the superconducting plane induced by two magnetic dipoles when $m_z/m_0 = 18$. (b) The z-component of the magnetic field $B_z(x, y = 0, z = 0)$ in the superconducting plane induced by two magnetic dipoles. A magnetic dipole is located at site (-3, 0, 2), and another is located at site (3, 0, 2).

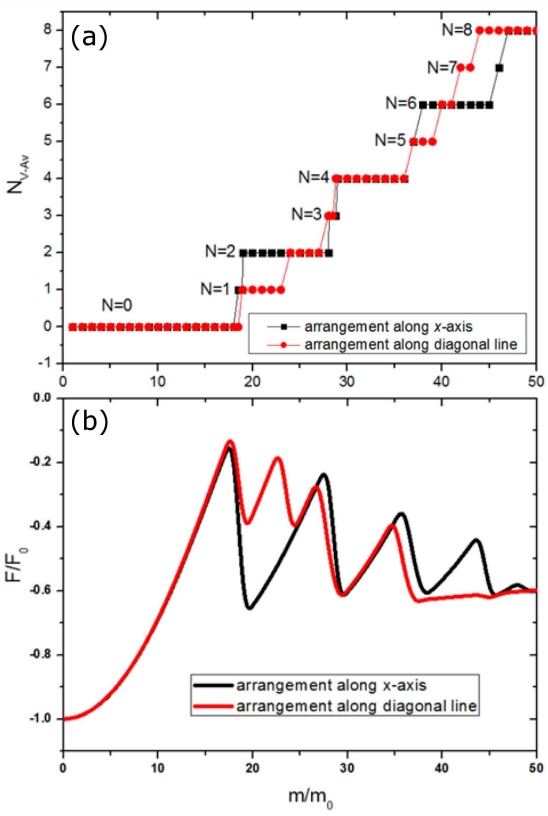

Fig. 3. (a) Number of V-Av pairs as a function of magnetic moments of two magnetic dipoles without applied magnetic field. Different lines with symbols represent the dependence for different arrange of two magnetic dipoles. (b) Free-energy as a function of magnetic moments of two magnetic dipoles without applied magnetic field.

to $N_{V-Av} = 8$ (Fig. 3a). As we can see from the Fig. 3a, the influence of boundary on the V–Av is enhanced when $m_z/m_0 > 38$. The corresponding free energy curves can be observed in the Fig. 3b. With increasing magnetic moment, the energy barrier for vortex entry becomes small and vortices and antivortices can penetrate the system. From the Fig. 3, We could derive the critical value of the dipole moment for the first appearance of a V–Av pair: $m/m_0 = 18$ for the arrangement along the x-axis and $m/m_0 = 19$ for the arrangement along the diagonal line.

Figure 4 shows the Cooper pair density, magnetization, and phase distribution for the arrangement along the diagonal line and along the x-axis, respectively. The magnitudes of the external magnetic field and magnetic moment are the $H/H_{c2} = 0.2$ and $m/m_0 = 30$, respectively. In the color scale, blue to red represent low to high for the Cooper pair density (z-axis) and $-\pi$ to π for the phase. We can see four vortices and four antivortices appearing in the superconducting film for the two arrangements of magnetic dipoles when the $H/H_{c2} = 0.0$ and $m/m_0 = 30$ (see the Fig. 3a). The four vortices were merged into a giant-vortex and the four antivortices were merged into a giant-antivortex. When the external magnetic field was introduced ($H/H_{c2} = 0.2$), the previous balance between vortices and antivortices was broken. Therefore, one new vortex configuration must be constructed in order to re-establish the dynamic balance of the interaction between vortices and antivortices. From the Fig. 4, we can see that the new vortex configuration consists of four vortices (merged into a giant-vortex) and four antivortices (merged into a giant-antivortex) for the arrangement along the diagonal line, and while four vortices (merged into a giant-vortex) and three antivortices (merged into a giant-antivortex) for the arrangement along the x-axis. To determine which correspond to vortices and which to antivortices it is convenient to look at the phase of the order parameter, depicted in the Fig. 4c and 4f. The phase changes clockwise from blue to red around 'usual' vortices while it goes counterclockwise around antivortices. Meanwhile, the Fig. 4b and e gives the direction of the supercurrent

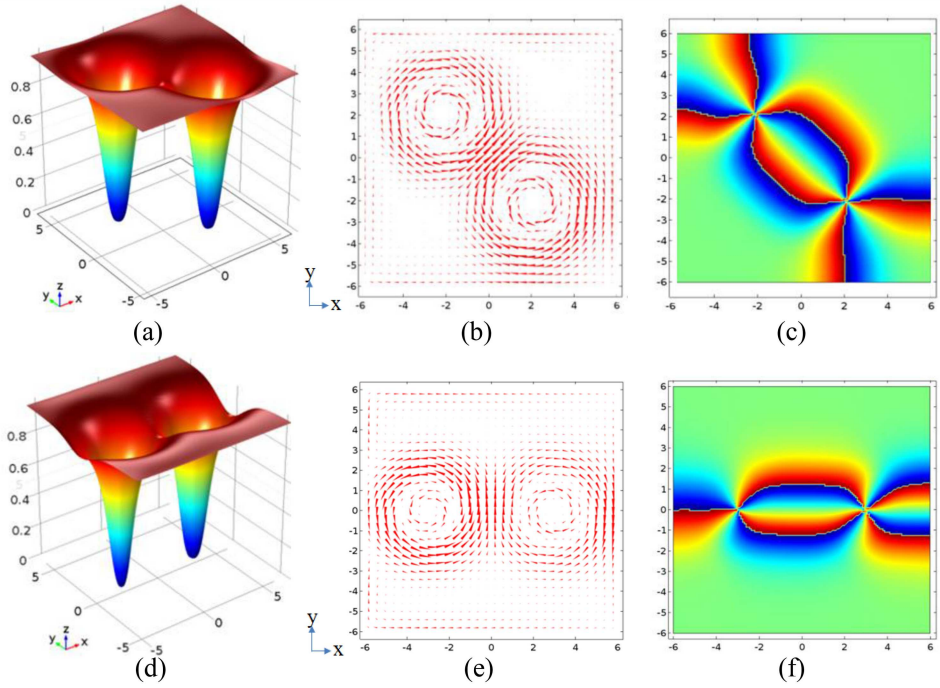

Fig. 4. (a)–(c) Cooper pair density, supercurrent and phase distribution for the arrangement along the diagonal line, respectively; (d)–(f) Cooper pair density, supercurrent and phase distribution for the arrangement along the x-axis, respectively. The magnitudes of the external magnetic field and magnetic moment are the $H/H_{c2} = 0.2$ and $m/m_0 = 30$. In the color scale, blue to red represent low to high for the Cooper pair density (z-axis) and $-\pi$ to π for the phase. The phase changes clockwise from blue to red around 'normal' vortices while it goes counterclockwise around antivortices.

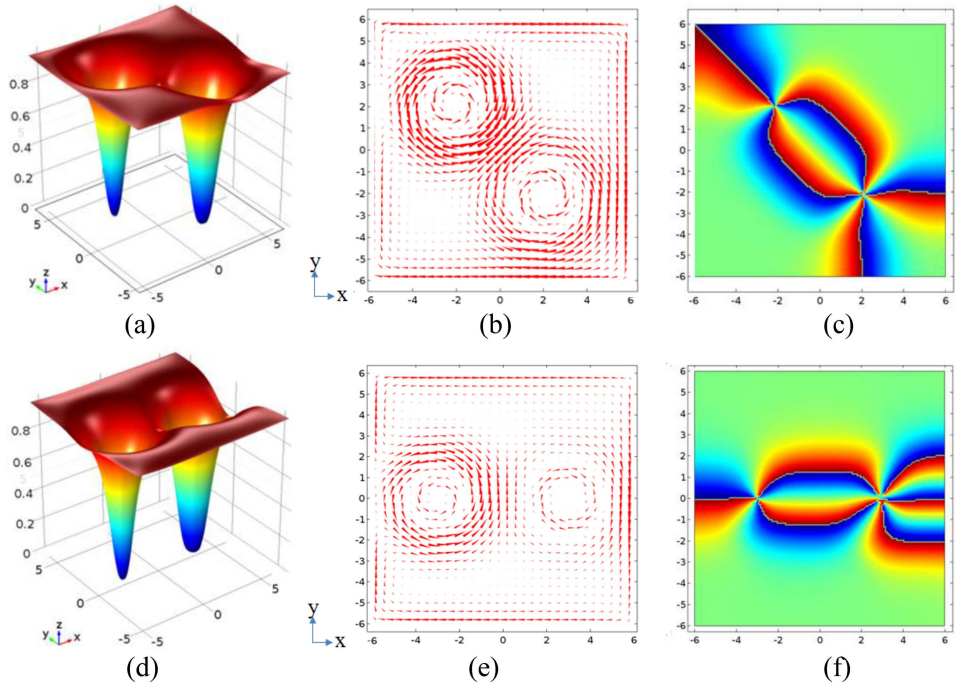

Fig. 5. (a)–(c) Cooper pair density, supercurrent and phase distribution for the arrangement along the diagonal line, respectively; (d)–(f) Cooper pair density, supercurrent and phase distribution for the arrangement along the x-axis, respectively. The magnitudes of the external magnetic field and magnetic moment are the $H/H_{c2} = 0.4$ and $m/m_0 = 30$, respectively. In the color scale, blue to red represent low to high for the Cooper pair density (z-axis) and $-\pi$ to π for the phase. The phase changes clockwise from blue to red around 'normal' vortices while it goes counterclockwise around antivortices.

and shows the antivortex has currents rotating in the opposite direction. The results of the Fig. 4 show that the coexistence of vortices and antivortices could occur in the mesoscopic superconducting-film due to the important influence of the magnetic diploes. And the formation and annihilation of the vortices and antivortices could be tuned and guided by the external magnetic field and the boundary feature. With increasing external magnetic field ($H/H_{c2} = 0.4$), we can observe that the new vortex configuration consists of four vortices (merged into a giant-vortex) and three antivortices (merged into a giant-antivortex) for the arrangement along the diagonal line (see the Fig. 5c), and while five vortices (merged into a giant-vortex) and three antivortices (merged into a giant-antivortex) for the arrangement along the x-axis (see Fig. 5f).

For comparison, we also consider a rectangle-shaped superconductor sample for the size of $L_x = 5\xi$ and $L_y = 11\xi$. Figure 6 shows the evolution of Cooper-pair density in a rectangle-shaped superconductor sample at the $H/H_{c2} = 0.3$, $I = 0.5I_0$, and $m/m_0 = 20$. Under the drive of the current vortex configurations reach to a stable state gradually. Compared with the case of the current $I = 0$, we observe four vortices and two antivortices, when the current $I = 0.5I_0$ (Fig. 7), which indicates that the injection of current prompts the information of vortices and antivortices.

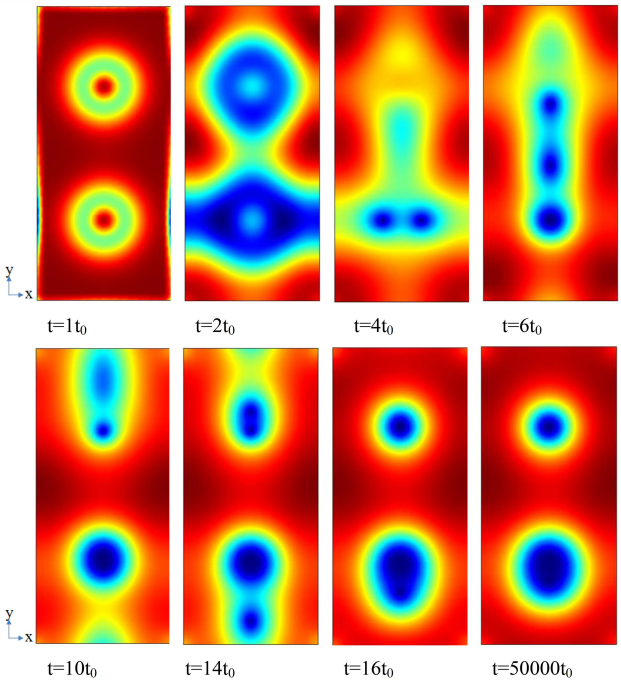

Fig. 6. Evolution of the Cooper-pair density in a rectangle-shaped superconductor sample at the $H/H_{c2} = 0.3$, $I = 0.5I_0$ and $m/m_0 = 20$.

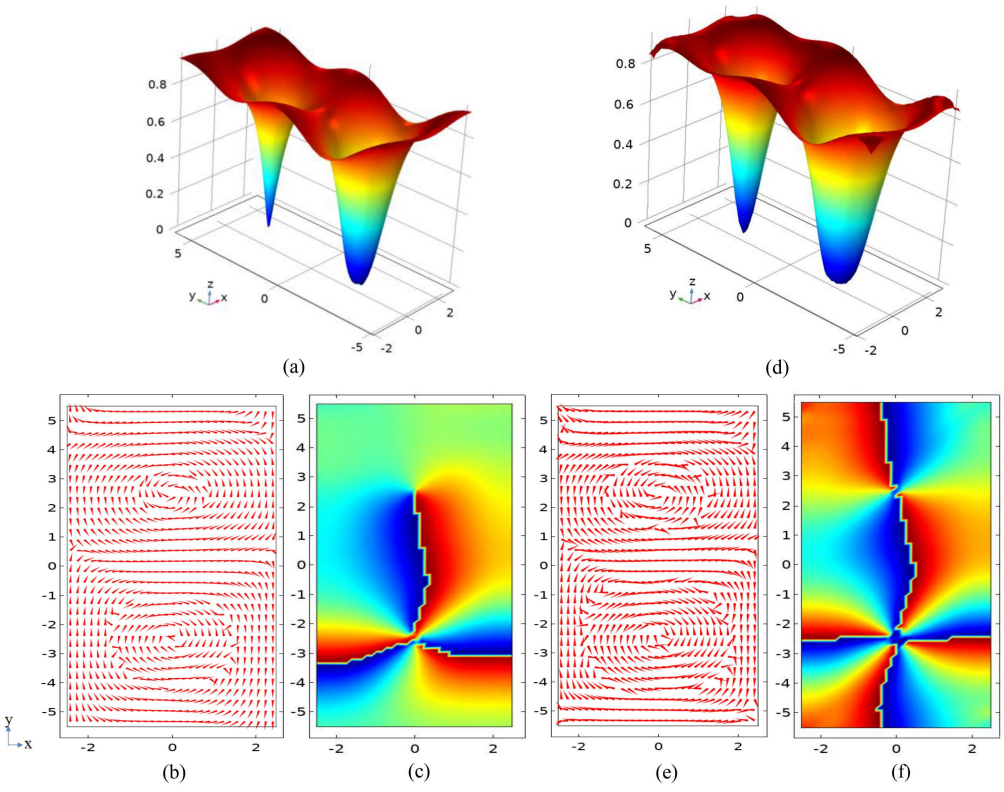

Fig. 7. (a–c) Cooper pair density, supercurrent and phase distribution for a rectangle-shaped superconductor sample at the $H/H_{c2} = 0.3$, $I = 0$ and $m/m_0 = 20$. (d–f) Cooper pair density, supercurrent and phase distribution for a rectangle-shaped superconductor sample at the $H/H_{c2} = 0.3$, $I = 0.5I_0$ and $m/m_0 = 20$, respectively. The current is injected from bottom to top. A magnetic dipole is located at site (0, 2.5, 2), and another is located at site (0, -2.5, 2).

4. Conclusions

In conclusion, we have studied in the framework of the time-dependent Ginzburg-Landau approach how the nonuniform magnetic field, created by the magnetic dipoles with a moment $\boldsymbol{m}$ and the applied magnetic field, penetrates into a mesoscopic superconducting film. We have derived the critical value of the dipole moment for the first appearance of a V–Av pair. Due to the joint action of the large magnetic moment of magnetic dipoles and the applied magnetic field, the diverse vortex-antivortex configurations could be generated inside a mesoscopic superconducting film. The magnetic dipoles also act as effective trapping centers for the vortices (or antivortices), causing an enhancement of vortex (or antivortices) pinning. The obtained results provide a tool for an effective manipulation of magnetic flux in mesoscopic hybrid structures and therefore could be potentially useful for application in fluxonics devices.

Acknowledgments

This work is sponsored by the Natural Science Foundation of Shanghai (No. 17ZR1411400, 16ZR1422700), the Science and Technology Commission of Shanghai Municipality (No. 14521102800), the National Natural Science Foundation of China (No. 51202141, 51672172), the Opening Project of Shanghai Key Laboratory of High Temperature Superconductors (No. 14DZ2260700).

References

[1] A.V. Kapra, V.R. Misko, D.Y. Vodolazov, F.M. Peeters, *Supercond. Sci. Technol.* **24**, 024014 (2011).

[2] M. Baert, V.V. Metlushko, R. Jonckheere, V.V. Moshchalkov, Y. Bruynseraede, *Phys. Rev. Lett.* **74**, 3269 (1995).

[3] V.V. Moshchalkov, M. Baert, V.V. Metlushko, E. Rosseel, M.J. Van Bael, K. Temst, R. Jonckheere, Y. Bruynseraede, *Phys. Rev. B* **54**, 7385 (1996).

[4] M.J. Van Bael, J. Bekaert, K. Temst, L. Van Look, V.V. Moshchalkov, Y. Bruynseraede, *Phys. Rev. Lett.* **86**, 155 (2001).

[5] M.V. Milošević, F.M. Peeters, *Phys. Rev. B* **69**, 104522 (2004).

[6] M.V. Milošević, F.M. Peeters, *J. Low Temp. Phys.* **139**, 257 (2005).

[7] M.V. Milošević, F.M. Peeters, *Phys. Rev. Lett.* **94**, 227001 (2005).

[8] M.V. Milošević, W. Gillijns, A.V. Silhanek, A. Libál, V.V. Moshchalkov, F.M. Peeters, *Appl. Phys. Lett.* **96**, 032503 (2010).

[9] M.V. Milošević, S.V. Yampolskii, F.M. Peeters, *Phys. Rev. B* **66**, 174519 (2002).

[10] M.M. Doria, *Physica C* **404**, 145 (2004).

[11] M.V. Milošević, F.M. Peeters, *Phys. Rev. Lett.* **93**, 267006 (2004).

[12] M.V. Milošević, F.M. Peeters, *Europhys. Lett.* **70**, 670 (2005).

[13] G.R. Berdiyorov, M.V. Milošević, F.M. Peeters, *Phys. Rev. B* **80**, 214509 (2009).

[14] J.S. Neal, M. V. Milošević, S. J. Bending, A. Potenza, L. San Emeterio, C.H. Marrows, *Phys. Rev. Lett.* **99**, 127001 (2007).

[15] M. Iavarone, A. Scarfato, F. Bobba, M. Longobardi, G. Karapetrov, V. Novosad, V. Yefremenko, F. Giubileo, A.M. Cucolo, *Phys. Rev. B* **84**, 024506 (2011).

[16] H.D. Gao, W.W. Sun, *J. Comput. Phys.* **294**, 329 (2015).

[17] Q. Du, *Phys. Rev. B* **46**, 9027 (1992).

[18] T.S. Alstrøm, M.P. Sørensen, N.F. Pedersen, S. Madsen, *Acta Appl. Math.* **115**, 63 (2011).

[19] Y. Jiao, L. Peng, Y. Zhu, L. Xu, Y. Wang, Y. Hu, Y. Zhou, *Acta Phys. Pol. A* **134**, 493 (2018).

[20] L. Peng, C. Cai, *J. Low. Temp. Phys.* **183**, 371 (2016).